

# Temperature and electric field dependence of ultrasonic wave propagation and attenuation in PZN-PT single crystal in vicinity of a phase transition

P. Hána · P. Bury · L. Burianova · S. J. Zhang ·  
T. R. Shrout · V. Ryzhenko

Received: 7 March 2007 / Accepted: 4 September 2007 / Published online: 12 October 2007  
© Springer Science + Business Media, LLC 2007

**Abstract** The longitudinal and transverse modes of ultrasound propagation in Lead Zinc Niobate–Lead Titanate (PZN–PT) single crystal solid solutions are investigated as a function of temperature. The influence of an electric DC bias field on the elastic stiffness at various temperatures is studied. The presence of more stable phases induced by this electric field is observed. The polarization directions are modeled in terms of free energy function. The experiments are conducted in a dedicated temperature chamber working in a wide temperature range from 200 up to 470 K for ultrasonic measurements thin plate samples with the option for DC bias fields. The bias field was applied by a high voltage amplifier Trek model 610D. Crystal cuts of [001], [110] and [111] were used for the study of electric field poling conditions and temperature influence on structure induced by polarization orientation. A study of anomalies in sound velocity and relative attenuation near ferroelectric transitions is performed. It is well established that near the temperature of a second-order structural phase transitions, and in particular near the Curie point of ferroelectrics, anomalously strong ultrasonic absorption occurs.

**Keywords** PZN–4.5%PT single crystal solid solution · Longitudinal and shear waves · Ultrasonic phase velocity and attenuation · Gibbs free energy · Structural phase transition

## 1 Introduction

In this article the propagation of ultrasound and the temperature dependence of ultrasound velocity in  $\text{Pb}(\text{Zn}_{1/3}\text{Nb}_{2/3})\text{O}_3$ –4.5%  $\text{PbTiO}_3$  (PZN–4.5%PT) single crystal solid solutions near the morphotropic phase boundary (MPB) is studied. An influence of an electric poling electric field to an unpoled sample on phase velocity is observed. The influence of phase and structural transitions on the phase velocity and relative attenuation is also investigated. An indirect ultrasonic observation of a rhombohedral-orthorombic phase transformation under [110] electric field loading can be determined. It is not necessary to measure the absolute attenuation of a sample because changes in relative attenuation as a function of temperature (acoustic spectrum) are of most interest [6]. For these measurements we use a pulse echo ultrasonic method [4, 5] with piezoelectric transducers (encapsulated and/or plates) working with frequencies up to 50 MHz [7]. We compare our results with the resonant measurements on thin plate PZN–4.5%PT <001> oriented sample. At this case the resonance frequency was approximately 29 MHz.

## 2 Samples

Three sample orientations we used for ultrasonic measurements, are given in Table 1 and Figs. 1, 2 and 3. Their thickness differed from 2 mm to smaller than 0.2 mm and

P. Hána (✉) · L. Burianova · V. Ryzhenko  
International Centre for Piezoelectricity Research,  
Technical University of Liberec,  
Liberec, Czech Republic  
e-mail: petr.hana@tul.cz

S. J. Zhang · T. R. Shrout  
Materials Research Institute, The Pennsylvania State University,  
University Park, PA 16802, USA

P. Bury  
Department of Physics, Faculty of Electrical Engineering,  
University of Zilina,  
010 26 Zilina, Slovak Republic

**Table 1** Sample orientations.

Sample cut orientation	Faces orientation
[100]	The three pair of faces are oriented in [100], [010] and [001]
[110]	The three pair of faces are oriented in [110], [ $\bar{1}\bar{1}0$ ] and [001]
[111]	The three pair of faces are oriented in [111], [ $\bar{1}\bar{1}0$ ] and [ $\bar{1}1\bar{2}$ ]

was the limiting parameter for the applicability of time of flight measurements with a transducer working on a fundamental frequency up to 20 MHz.

Various sets of plate samples with different thicknesses were used. The thicker ones (thickness 0.5 and 2.0 mm) were without electrodes and unpoled. The thinner ones with thickness 0.2–0.3 mm were coated by sputtered gold and poled by an electric field (10 kV/cm) at temperature 160°C higher than Curie temperature  $T_C=150^\circ\text{C}$  of PZN–4.5%PT composition for a few minutes and slowly cooled down with applied field. The velocity measurements were performed for all three samples at room temperature. The results are summarized in Table 2.

## 2.1 Theory

The polarization direction under an applied electric field and changing temperature conditions was simulated using Landau–Devonshire–Ginzburg (LGD) phenomenological theory. The Gibbs free energy is derived from  $m3m$  symmetry under isothermal conditions [1–3]:

$$\begin{aligned} \Delta G = & \alpha_1^x (P_1^2 + P_2^2 + P_3^2) + \alpha_{11}^x (P_1^4 + P_2^4 + P_3^4) \\ & + \alpha_{12}^x (P_1^2 P_2^2 + P_2^2 P_3^2 + P_3^2 P_1^2) \\ & + \alpha_{111}^x (P_1^6 + P_2^6 + P_3^6) \\ & + \alpha_{112}^x [P_1^4 (P_2^2 + P_3^2) + P_2^4 (P_1^2 + P_3^2) + P_3^4 (P_1^2 + P_2^2)] \\ & + \alpha_{123}^x P_1^2 P_2^2 P_3^2 - E \cdot \cos \alpha_i \cdot P_i \end{aligned} \quad (1)$$

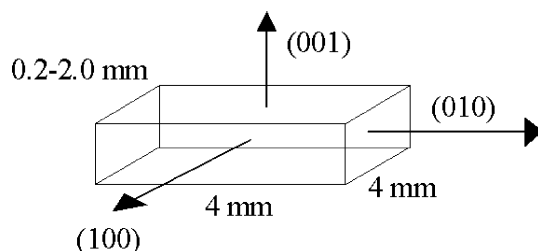


**Fig. 1** Sample of [001] direction and building engineered domain structure

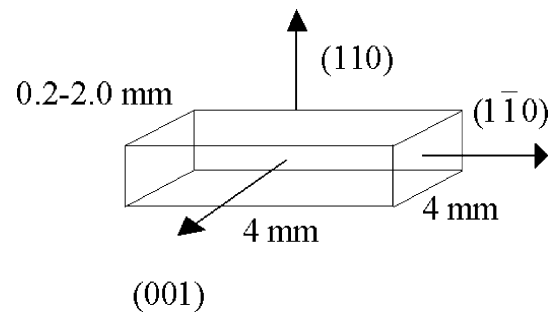


**Fig. 2** Sample of [110] direction and enforcing orthorhombic symmetry

where  $\alpha_{ij}^x$  are dielectric stiffness coefficients. The application of an electric field at a given direction is represented by directional cosines  $\cos \alpha_i$  in the last energy function term and  $E$  is the magnitude of the biasing electric field.

Dielectric stiffness coefficients were calculated using mixed rule [2] from parameters of end members solid solution PZN and PT (lead titanate). The values of stiffness coefficients are tabulated in Table 3.

## 2.2 Composition dependence

To study a binary solid solution system, we assumed the simple composition dependence of the coefficients. We applied linear functions for all coefficients  $\alpha_{i..}^x$  on composition:

$$\alpha_{i..}^x = (1 - x) \cdot \alpha_{i..}^a + x \cdot \alpha_{i..}^b$$

where  $x$  is the molar fraction of PT at PZN:PT solid solution system.

## 2.3 Simulation of the Gibbs potential

Table 3 gives a set of coefficients of the end members PZN–4.5%PT solid solution free energy function. This set is used for qualitative simulation of the temperature- and the field-dependent behavior of the binary system of 95.5% PZN–4.5% PT single crystal.

Figure 4 illustrates the main polarization directions following from energy function 1 for the system under investigation.

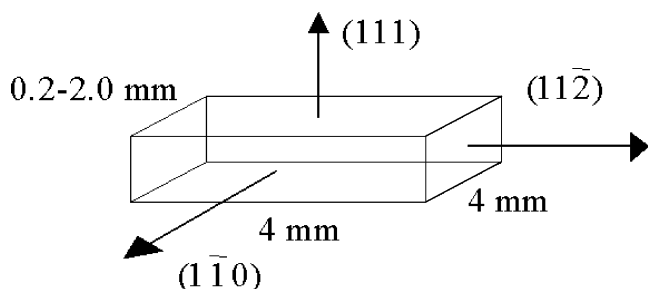


**Fig. 3** Sample of [111] direction and enforcing rhombohedral symmetry

**Table 2** PZN–4.5%PT samples at room temperature.

Sample cut	Velocity	Unpoled <sup>a</sup> $v$ (m/s)	Poled <sup>b</sup> $v$ (m/s)	Partly repoled <sup>c</sup> $v$ (m/s)	High field <sup>d</sup> $v$ (m/s)
001	Transverse mode	3618±8	4100±2	4100±8	4113±5
	Longitudinal mode	2710±2	2732±2	2732±5	2747±5
110	Longitudinal mode	4595±2	4800±2	4513±5	4800±2
	Transverse mode	2739±2	2725±10	2725±10	2726±5
111	Transverse mode	4690±5	4818±2	4818±2	4828±2

<sup>a</sup> Virgin samples without applied electric field<sup>b</sup> Samples with applied electric field exceeding coercivity for a limited time<sup>c</sup> Samples with applied negative electric field smaller than coercivity one for a limited time<sup>d</sup> Samples with biasing electric field

## 2.4 Experimental set-up

### 2.4.1 Temperature and electric field bias measurements

Temperature measurements were realized in a special sample holder plotted in Fig. 5. The temperature of the sample is set by direct contact with copper thick plate heated resistively and a cooling pipe on the bottom with an exhaust of nitrogen vapors on the sample. The metal plate serves as the ground electrode, too. The temperature range of stabilization is approximately –100°C to 300°C with an absolute accuracy ±0.1°C and with a resolution better than ±0.01°C.

Electric field measurements were realized in the same sample holder given in Fig. 5. A thin aluminum foil is placed between the sample and the quartz delay line providing good electric and acoustic contact. The slot around the sample is filled by silicon oil to prevent breakdown on the outside edges of the sample.

## 2.5 Polarization measurement

We have realized measurements of an unpoled sample of PZN–4.5%PT cut [110] direction, see Fig. 6. We observed three states characterized by various ultrasound velocities. The first state is the case of an unpoled sample characterized with rhombohedral microsymmetry, see Fig. 4, with random distribution of eight possible polarization directions.

Macroscopic polarization is achieved by applying a sufficiently high electric fields along the [110] direction and induces a stable orthorhombic symmetry with one preferred domain state. This situation is demonstrated by the energy function plot in Fig. 7.

Horizontal axes represent plane given by [110] and [001] direction of polarization. On vertical axes the energy is given in standard units (J). It means the figure represent the minimum potential energy along the [110] direction with a polarization minimum at 0.408 C/m<sup>2</sup>.

During the repolarization process a metastable phase occurs with rhombohedral symmetry and a polarization minimum of 0.425 C/m<sup>2</sup> lying along the [111] direction, see Fig. 8, with two possible preferred domain states as it follows from Fig. 4. The longitudinal velocity 4,513 m/s in Fig. 8 characterizes this induced symmetry.

The application of a sufficiently high electric field tends to polarize the sample again and stabilizes the orthorhombic symmetry with a polarization minimum at 0.408 C/m<sup>2</sup> with a longitudinal velocity 4,800 m/s, see Figs. 6 and 8, with one stable domain again as follows from Fig. 4.

## 2.6 Temperature-dependent measurements

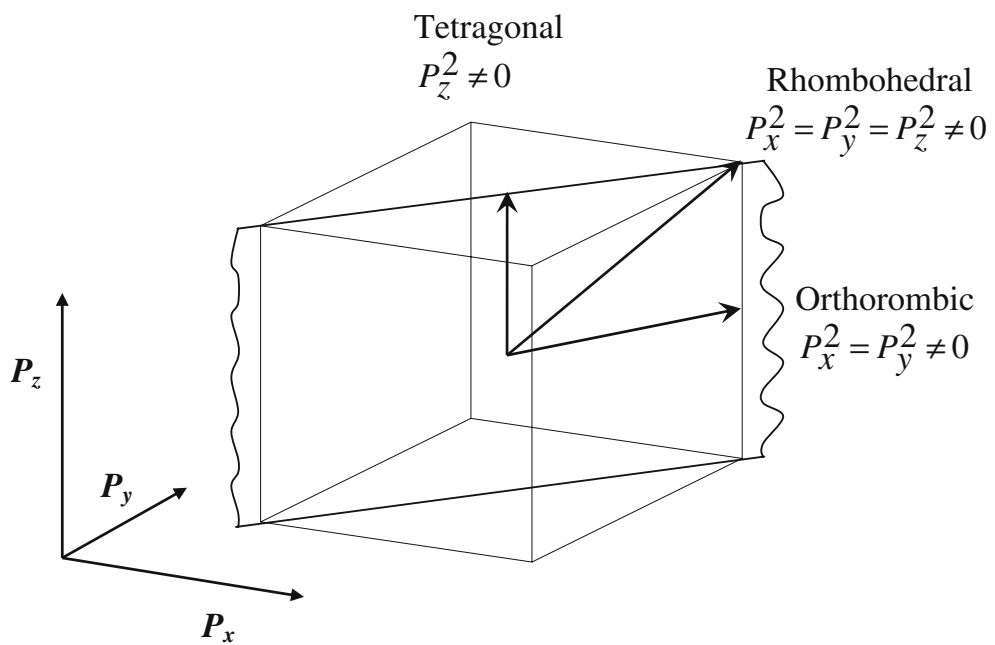
In Figs. 9 and 10 the temperature dependence of the longitudinal wave velocity is plotted for the unpoled samples. The rate of heating was 1 K/min. Four regions in the temperature range from up to are observed with various tangents of linear dependence. The impact of the crystal orientation is also observed by the temperature-dependent behavior of ultrasound propagation. In Figs. 9 and 10 we can see different behavior of longitudinal ultrasound waves propagating in two different directions.

On both figures are well visible structural ferroelectric phase transitions from the rhombohedral to the tetragonal symmetry at a temperature of approximately 120°C. A paraelectric phase transition is observed at about 150°C. Figure 10 shows a process of polarization rotation through monoclinic phases into a tetragonal state. The different behavior of ultrasound longitudinal wave propagation is

**Table 3** PZN and PT dielectric stiffness coefficients.

PZN	PT
$\alpha_1^q(t) = 4.74 \cdot 10^5 \cdot (t - 130)$	$\alpha_1^b(t) = 1.51 \cdot 10^5(t - 475.9)$
$\alpha_{11}^q = -1.40 \cdot 10^8$	$\alpha_{12}^q = -2.03 \cdot 10^8$
$\alpha_{111}^b = 2.13 \cdot 10^9$	$\alpha_{112}^q = 2.79 \cdot 10^9$
$\alpha_{111}^q = 1.41 \cdot 10^9$	$\alpha_{111}^b = 2.13 \cdot 10^9$
$\alpha_{112}^q = 2.79 \cdot 10^9$	$\alpha_{112}^b = 5.00 \cdot 10^9$

**Fig. 4** Polarization directions for various phases



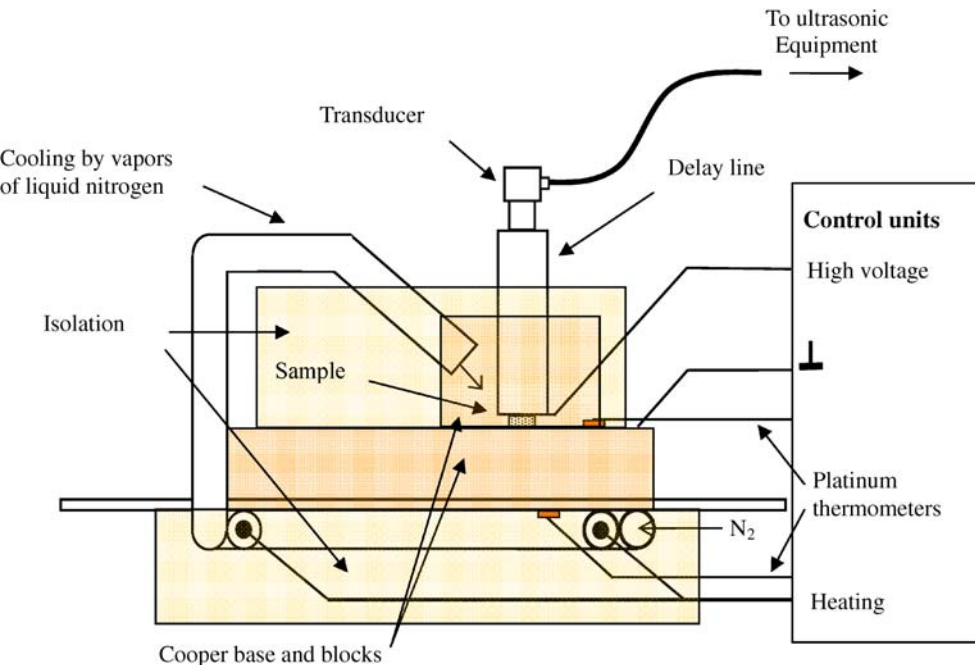
simply given by the direction of propagation with regard to the polarization direction.

Figure 10 illustrates the measurement of the longitudinal wave velocity for a sample cut along the [111] direction under equivalent conditions. We can observe the same regions as for a cut along the [110] direction.

## 2.7 Attenuation measurements

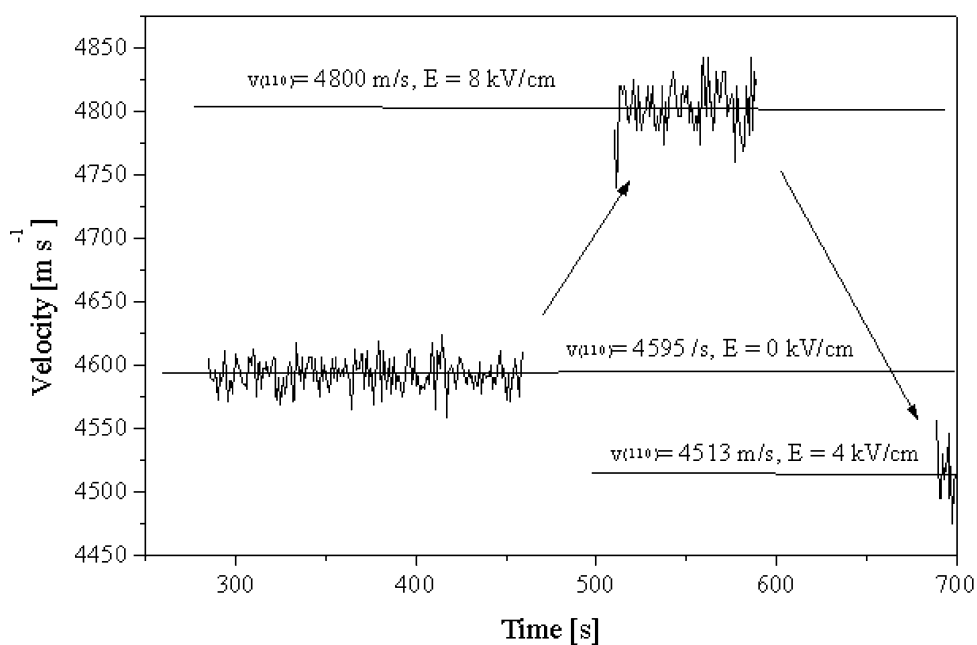
The attenuation measurements of thin poled samples exhibit a more detailed structure than velocity measurements. Heating and cooling rates of 0.25 K/min were used. Figure 11 illustrates the attenuation spectrum measured at

**Fig. 5** Temperature chamber for electric field dependence ultrasonic measurements



**Fig. 6** The presence of three stable crystal phases

PZN-4.5%PT <110> Switching unpoled rhombohedral - orthorombic - rhombohedral



29 MHz using a longitudinal acoustic wave registered during the cooling of the sample. There are two presumed peaks temperatures of 131.7°C and 150.9°C in the attenuation spectrum. Peaks represent ferroelectric phase

transition from rhombohedral to tetragonal symmetry and the paraelectric phase transition into the parental cubic symmetry. We also identify another peak at 104.4°C that can be associated with the domain structure of the

**Fig. 7** The induced orthorhombic symmetry by high electric field in direction [110]

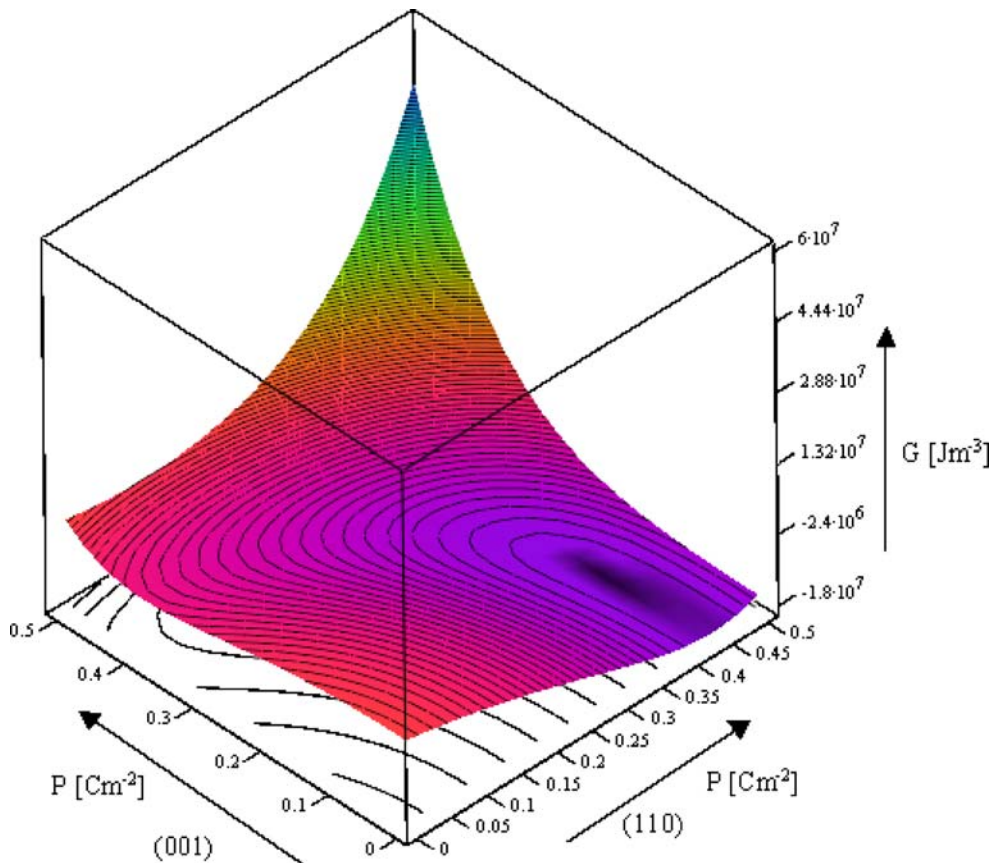


**Fig. 8** The rhombohedral symmetry at room temperature with low electric field in direction [110]

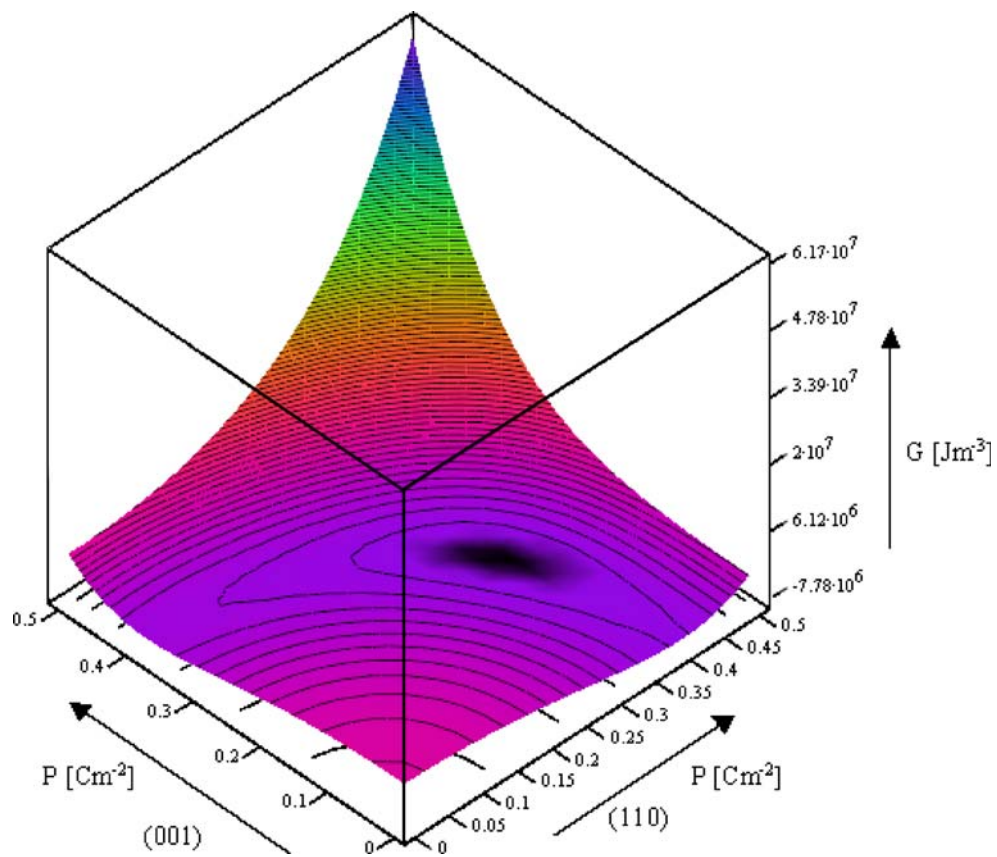


**Fig. 9** Temperature dependence of longitudinal wave velocity of the [110] cut

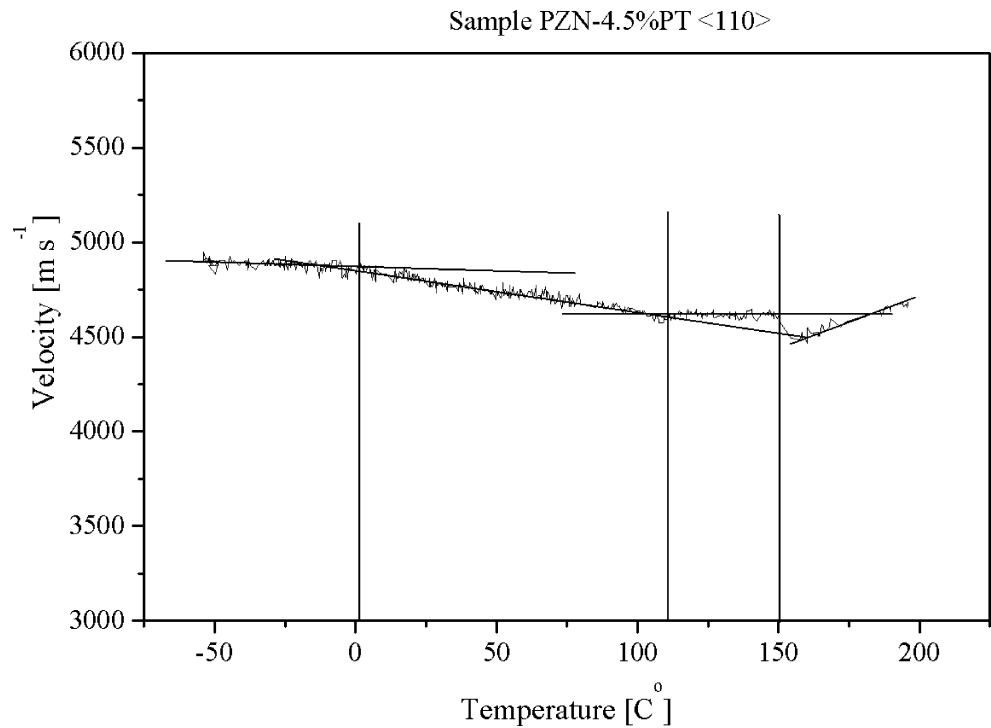
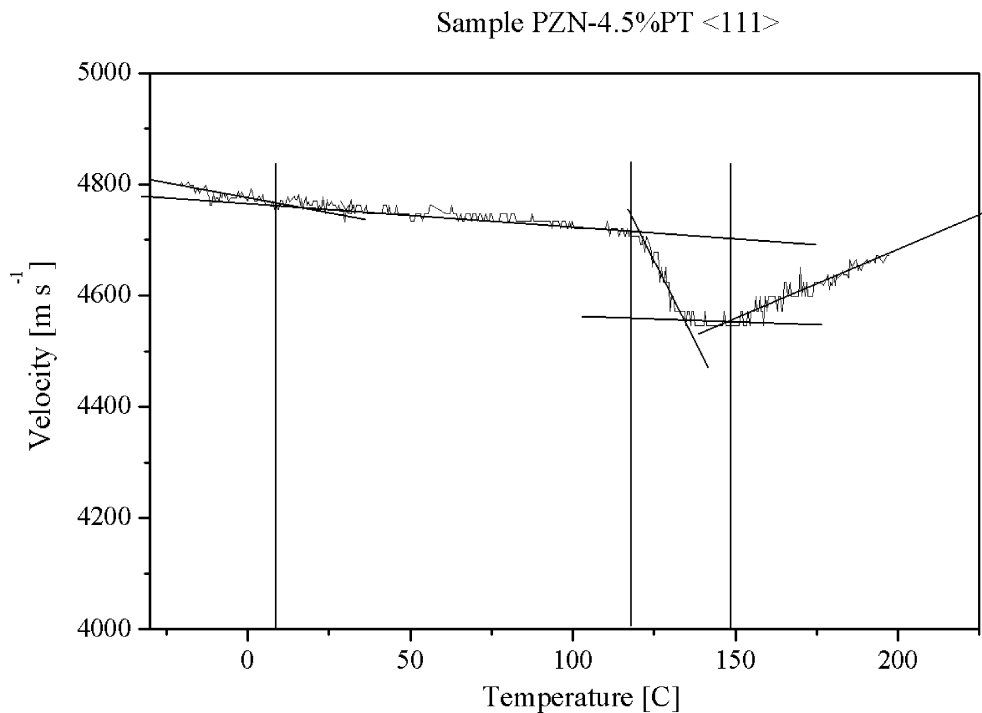


**Fig. 10** Temperature dependence of longitudinal wave velocity of the [111] cut



ferroelectric phase. The rate of the longitudinal waves measured by that method is approximately 3,480 m/s at room temperature. The following Fig. 12 for heating exhibits shifted and slightly blurred peaks.

### 3 Discussion

The low temperature ( $\approx 10^{\circ}\text{C}$ ) change in phase velocity temperature dependence in Figs. 9, 10 and 11 can be attributed to the existence of a monoclinic phase mixed with

a rhombohedral one At higher temperatures we can observe a structural transition from rhombohedral to tetragonal crystal symmetry and a phase transition from the ferroelectric phase and tetragonal symmetry to the paraelectric phase represented by the parental cubic symmetry.

The effect of the electric field applied to unpoled samples suggests the existence of more stable structures. In the case of a sample cut along <110> we induce structures with rhombohedral symmetry, two possible polarization directions, at low applied electric fields and orthorhombic symmetry with one polarization direction for high electric fields.

**Fig. 11** Temperature dependence of longitudinal wave attenuation of the [001] cut during cooling

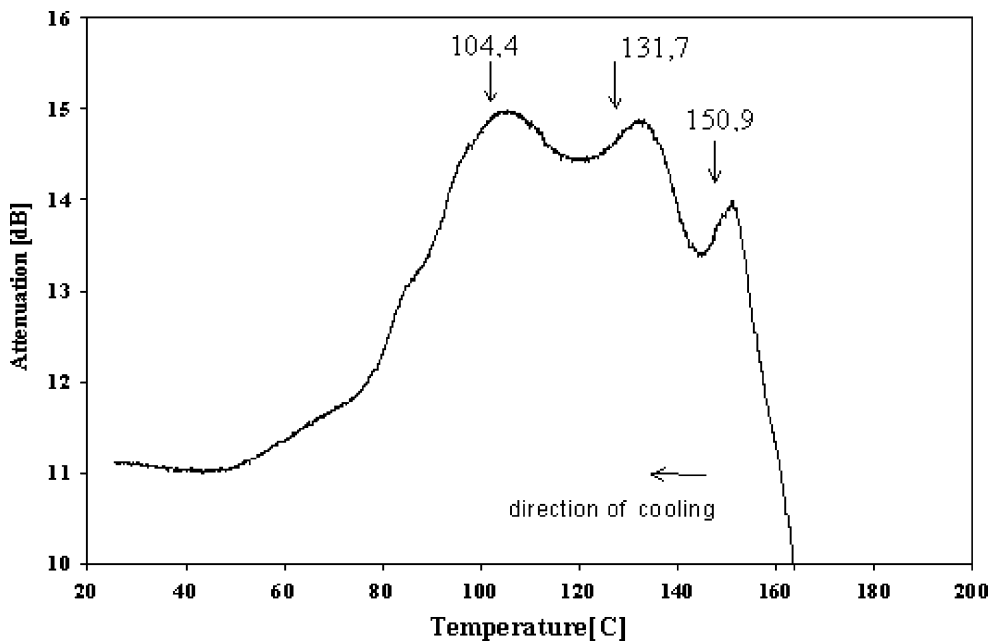
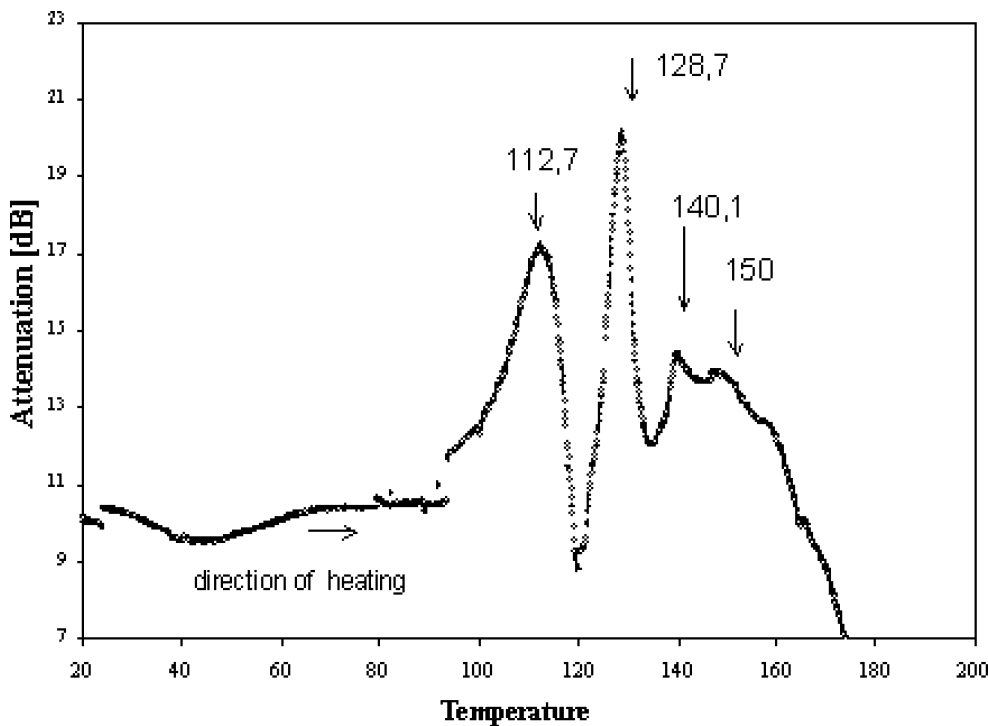


**Fig. 12** Temperature dependence of longitudinal wave attenuation of the [001] cut during heating



The physics of the transitions and phase stability can be examined not only from the perspective of the free-energy analysis given by a thermodynamic approach but also with respect to the microscopic details of lattice dynamics and to macroscopic ferroelastic domain states. The presence of an orthorhombic phase was deduced by electric bias field measurements.

The more complex shape of temperature dependence of ultrasonic attenuation can be caused by the influence of mixed phase states and complex domain structure, which can induce various phases. To verify the influence of the domain structure on the probability of an induced phase we performed poling of the samples and measurements with an applied electric bias.

#### 4 Conclusion

Ultrasonic study of single crystal systems near MPB enables to observe both structural stability and phase transitions. The velocity and the attenuation measurements allow us to accurately study domain states and/or existence of more stable phases. and their evolution

versus field and temperature. The attenuation measurement exhibits extremely high sensitivity to structure changes but the explanation of this behavior directly connected to microscopic structure is more complex. It is necessary to use additional experimental methods to describe this behavior.

**Acknowledgments** This work was supported by the Grant Agency of the Czech Republic (GA ČR 202/07/1289).

#### References

1. S. Stotz, Ferroelectrics **76**, 123 (1987)
2. K. Abe, O. Fukurava, H. Imagawa, Ferroelectrics **87**, 55–64 (1988)
3. M.J. Haun, E. Furman, S.J. Jang, L.E. Cross, Ferroelectrics **99**, 63–86 (1989)
4. H. Kamioka, Jpn. J. Appl. Phys. **36**, 2896–2901 (1997)
5. J. Yin, W. Cao, J. Appl. Phys. **92**(1), 444–448 (2002)
6. P. Hana, L. Burianova, E. Furman, L.E. Cross, Ferroelectrics **293**, 321–330 (2003)
7. P. Hana, L. Burianova, E. Furman, S. Zhang, T.R. Shrout, V. Ryzhenko, P. Burry, Ferroelectrics **319**, 371–380 (2005)